의학 석사 학위논문

Trimethyltin-induced microglial activation and its mechanisms in BV-2 cells

Trimethyltin에 의한 미세아교세포주 BV-2 cell의 활성화와 그 기전

2015 년 8 월

서울대학교 대학원

의학과 약리학 전공

김 다 정

A Thesis of Master's Degree in Medical Science

Trimethyltin-induced microglial activation and its mechanisms in BV-2 cells

Trimethyltin에 의한 미세아교세포주 BV-2 cell의 활성화와 그 기전

August 2015

Graduate School of Seoul National University
College of Medicine

Medical Science (Pharmacology)

Da Jung KIM

Trimethyltin에 의한 미세아교세포주 BV-2 cell의 활성화와 그 기전

지도 교수 김 용 식

이 논문을 의학석사 학위논문으로 제출함
2015 년 4 월

서울대학교 대학원
의학과 약리학 전공
김 다 정

김다정의 의학석사 학위논문을 인준함
2015 년 6 월

위 원 장 김 혜선 (인)

부위원장 김 용식 (인)

위 원 윤 인희 (인)

Trimethyltin-induced microglial activation and its mechanisms in BV-2 cells

Advising progessor Yong Sik KIM

Submitting a master's thesis of Public Administration

April 2015

Graduate School of Seoul National University
College of Medicine
Medical Science (Pharmacology)

Da Jung KIM

Confirming the master's thesis written by
Da Jung KIM
June 2015

Professor _____ Chairman

Professor _____ Vice Chairman

Professor _____

Abstract

Trimethyltin (TMT) is known as a potent neurotoxicant that causes neuronal cell death and neuropathological symptoms. The precious mechanism of TMT toxicity is still not fully understood, however, reactive oxygen species (ROS), microglial activation and recruitment of inflammatory mediators are considered to play a crucial role in the process. Microglial activation is one of the prominent pathological features of TMT neurotoxicity, despite, a limited number of studies have been reported on how microglial activation occurs in TMT intoxication. In this study, we aimed to investigate signaling pathways by which microglial activation is induced by TMT. By using BV-2 murine microglial cells, TMT-induced ROS generation, mitogen-activated protein kinases (MAPKs) and nuclear factor-κB (IκBα phosphorylation inhibitor) signaling and pro-inflammatory mediators were examined. Additionally, the effect of TMT-induced microglial activation on neuronal cell survival was examined in a co-culture with HT22 neuroblastoma cells. As a result, TMT generated ROS and increased the expression of CD11b and NF-κB-mediated nitric oxide (NO) and tumor necrosis factor (TNF)-α in BV-2 cells. We also observed that NF-κB activation was controlled by p38 and JNK phosphorylation. Moreover, TMT-induced ROS generation occurred via nicotinamide adenine dinucleotide phosphate (NADPH) oxidase in these cells. Interestingly, pretreatment with the NADPH oxidase inhibitor apocynin significantly suppressed p38, JNK, and NF-κB activation and ultimately the production of pro-inflammatory mediators upon

TMT exposure. These findings indicate that NADPH oxidase-dependent ROS generation activated p38 and JNK MAPKs, which then stimulated NF-κB to release pro-inflammatory mediators in the TMT-treated BV-2 cells. In the co-cultured system, the activation of the microglia by TMT caused the death of the HT22 cells and it was significantly rescued by pretreatment of apocynin, SB203580 (p38 inhibitor) or SP600125 (JNK inhibitor). These results suggest that TMT-generated ROS and pro-inflammatory factors might cooperate to mediate neuronal death. Taken together, TMT could directly activate microglia to become deleterious to neuronal cell survival.

Keywords : BV-2 microglial cells, HT22 neuroblastoma cells, mitogen-activated protein kinases (MAPKs), NADPH oxidase, nuclear factor-κB (NF-κB), trimethyltin (TMT)

Student Number : 2013-21720

Contents

List of figures

List of Abbreviations

iNOS, Inducible nitric oxide synthase

MAPKs, Mitogen-activated protein kinases

NADPH, Nicotinamide adenine dinucleotide phosphate

NF-κB, Nuclear factor -κB

NO, Nitric oxide

ROS, Reactive oxygen species

TMT, Trimethyltin

TNF-α, Tumor necrosis factor -alpha

Introduction

Organotin compounds, particularly di- and tri-alkyl tins, are used as stabilizers in polyvinyl chloride (PVC) and as biocides (Furuhash et al. 2008). Poisoning accidents involving these compounds have been reported (Tang et al. 2013). Trimethyltin (TMT) is known to be highly neurotoxic compared to other organotin compounds. Human exposure to TMT causes neuropathological symptoms, cognitive impairments, hyperactivity, aggressive behavior and seizures (Furuhash et al. 2008; Yoo et al. 2007). These clinical symptoms are closely related to limbic system dysfunction in the brain (Geloso et al. 2011). In rodent models, TMT administration induces massive neuronal cell loss with glial reactivity in the brain and behavioral alternations that include cognitive impairments, hyperactivity and tonic-clonic seizures (Geloso et al. 2011, McPherson et al. 2011; Noraberg et al. 1998). However, the precise mechanism governing its neurotoxicity remains unclear. Thus far, the suggestions regarding TMT-induced neurotoxic mechanisms include calcium overload (Geloso et al. 2011), excitotoxicity (Gunasekar et al. 2001), mitochondrial dysfunction (Noraberg et al. 1998), oxidative stress (Geloso et al. 2011; Noraberg et al. 1998) and neuroinflammation (McPherson et al. 2011; Viviani et al. 1998). Among these neurotoxic mechanisms, neuroinflammation has recently emerged as a key player because extensive glial activation and pro-inflammatory cytokine production are accompanied by neuronal death in many neurodegenerative disorders (Nilsberth

et al. 2002; Minghetti et al. 2005).

In the central nervous system (CNS), microglia are the resident macrophage-like cells and play an important role in immune function (Henn et al. 2009). Lipopolysaccharide (LPS) (Liu et al. 2011; Xing et al. 2011) and various neurotoxins such as amyloid beta (Aβ) (Bachstetter et al. 2011; He et al. 2011), 1-methyl-4-phenyl-1,2,3,6-tetrahydropyridine (MPTP) (Lull and Block 2010) and rotenone (Gao et al. 2013) can activate microglia to release cytotoxic factors, such as superoxide (O_2^-), nitric oxide (NO), tumor necrosis factor (TNF)-α, and interleukin (IL)-1β (Lull and Block 2010; Ransohoff and Perry 2009), factors that reliably trigger neuronal death (Lull and Block 2010; Wakselman et al. 2008). The proinflammatory products from activated microglia are generally known to appear via mitogen-activated protein kinases (MAPKs) and the NF-κB pathway (Park et al. 2012; Peterson and Flood 2012). The association between neuroinflammation and microglial activation was elucidated by studies in AD (Nilsberth et al. 2002), Parkinson's disease (Minghetti et al. 2005) and multiple sclerosis (Akiyama et al. 2000).

The administration of TMT to rodents induces early, pronounced glial reactivity with neuronal death and the enhancement of inflammatory factors including TNF-α, IL-1β, IL-12, IL-23 and NO in the hippocampus (McPherson et al. 2011; Noraberg et al. 1998). Previously, it was reported that

amoeboid microglia with elevated mRNA levels of pro-inflammatory factors, such as TNF-α and macrophage inflammatory protein (MIP)-1α, were detected at an early time point after TMT treatment (d'Hellencourt and Harry 2005). In the rat hippocampal slice culture (Noraberg et al. 1998) and mixed neuronal cultures (Fiegel and Dzwonek 2007), selective microglial changes prior to any sign of neuronal damage have been reported. Moreover, the microglial activation induced by TMT potentiates neuronal cell death in a co-culture of neurons with microglia (Eskes et al. 2003). Similarly, it has also been reported that TMT can evoke microglial activation in co-cultures of microglia with astrocytes (Röhl and Sievers 2005; Röhl et al. 2009). These *in vitro* and *in vivo* studies indicate the importance of cell-to-cell interactions, particularly between microglia and neurons and between microglia and astrocytes in TMT-induced neuroinflammatory reactions (Eskes et al. 2003; Geloso et al. 2011; McPherson et al. 2011).

However, the direct effect of TMT on microglial cells *in vitro* has not been previously evaluated. Some controversial reports state that TMT either does not directly activate (Röhl and Sievers 2005; Röhl et al. 2009) or partially activates microglia (Viviani 1998) with or without any significant morphological changes in microglia-enriched culture (Eskes et al. 2003; Reali et al. 2005); however, most of these previous reports have demonstrated that the microglial activation induced by TMT is potentiated in co-culture conditions with neurons (Eskes et al. 2003) or astrocytes (Röhl and Sievers 2005; Röhl et al. 2009;

Viviani et al. 1998). Additionally, few studies have examined the underlying mechanism of microglial activation induced by TMT. From this background, we sought to evaluate whether TMT can directly activate microglia and the identities of the cellular mechanisms that are involved in this process using BV-2 microglial cells. Furthermore, we also examined the role of TMT-induced microglial activation on neuronal cell death in a co-culture system with HT22 neuroblastoma cells.

Materials and Methods

Reagents

Dulbecco's modified Eagle's medium (DMEM), phosphate-buffered saline (PBS), Hank's-balanced salt solution (HBSS), fetal bovine serum (FBS), normal goat serum (NGS) and antibiotic-antimycotic 100X were purchased from Gibco (Grand Island, NY, USA). Trimethyltin chloride, 2,7-dichlorofluorescin diacetate (DCFH-DA), 1-(4,5-dimethylthiazol-2-yl)-3,5-diphenylformazan (MTT), dimethyl sulfoxide (DMSO), bovine serum albumin (BSA), Tween-20, Hoechst 33258, SB203580, SP600125, apocynin, and BAY11-7082 were from Sigma-Aldrich (St. Louis, MO, USA). Rabbit antibodies against p-JNK, p-p38, p-ERK, p-IκBα, p38, and IκBα were purchased from Cell Signaling Technologies, Inc. (Beverly, MA, USA). Rabbit anti-JNK, ERK and NF-κB p65 antibodies were from Santa Cruz Biotechnology (Santa, CA, USA). Mouse anti-inducible nitric oxide synthase (iNOS) was from BD Biosciences (Franklin Lakes, NJ, USA). Mouse anti-actin was purchased from EMD Millipore (Billerica, MA, USA). Rat anti-CD11b was from AbD Serotec (Oxford, UK). The goat anti-mouse, rabbit and rat IgG (HRP-conjugated) secondary antibodies were from Enzo Life Science (Farmingdale, NY, USA). All other chemicals were purchased from Sigma-Aldrich.

Cell culture and treatment

The BV-2 cells were maintained at 36℃ in a 5% CO_2 incubator with high-glucose DMEM supplemented with 10%

(v/v) FBS, 1x antibiotic-antimycotic (consisting of 100 units/ml penicillin, 100 μg/ml streptomycin, and 0.25 μg/ml amphotericin B), 2 mM L-glutamine, and 1 mM pyruvate at pH 7.4. At 80% confluence, cells were harvested for subculture. The cells were seeded on a plate and incubated overnight in the culture medium containing 10% (v/v) heat-inactivated FBS and antibiotics. For the western blot, ROS measurement and immunocytochemistry experiments, the media were then replaced with low-glucose DMEM without FBS and antibiotics and incubated for at least 4 hr prior to various inhibitor treatments. For all of the inhibitors, including SB203580 (p38 MAPK inhibitor), SP600125 (JNK MAPK inhibitor), apocynin (nicotinamide adenine dinucleotide phosphate [NADPH] oxidase inhibitor) and BAY11-7082 (IκBα phosphorylation inhibitor) and the vehicle control (0.1% DMSO), the pre-treatments lasted 1 hr, and TMT dissolved in saline was then added to the culture media for the indicated times.

Cell viability –MTT Assay

To determine the survival of the BV-2 cells upon TMT exposure, 1.5 x 10^4 cells were seeded in each well of a 96-well tissue culture plate (BD, Franklin Lakes, NJ, USA). After sitting overnight, the cells were gently washed with PBS (pH 7.4) twice, and the medium was replaced with low-glucose DMEM medium with 1% (v/v) FBS. Various concentrations of TMT were applied to the BV-2 cells. After 24 hr of incubation, the medium was removed, and the MTT solution (final concentration, 0.5 mg/ml) was added. Following 3 hr of

incubation in a CO_2 incubator at 36℃, the MTT solution was aspirated, and 200 μl of DMSO was added to each well. The absorbances were then read with a microplate reader (Tecan infinite M200 Pro, Tecan, San Francisco, USA) at 495 nm. The absorbance of the control cells was set to 100%.

Measurement of ROS

Intracellular ROS generation was measured with dichlorofluorescein diacetate (DCFH-DA) assays (Yan et al. 2013). In 60-mm^2 tissue culture dishes (BD, Franklin Lakes, NJ, USA), the treated cells at a density of 1×10^6 cells/ml were washed twice with pre-warmed HBSS. Next, the cells were incubated with 15 μM DCFH-DA at 36℃ in a CO_2 incubator for 30 min. The cells were again washed twice. A Canto Flow Cytometer (BD Biosciences, CA, USA) was used to fluorescently quantify the cells (excitation at 488 nm and emission at 510 nm). To provide statistical data, the value measured for the control was set to 100%.

Western blot analysis

The treated cells were lysed with radioimmunoprecipitation assay (RIPA) buffer (Elpis Biotech, Daejeon, Korea) supplemented with protease and phosphatase inhibitor cocktails (Roche Diagnostics, Rotkreuz, Switzerland) and centrifuged at 14,000 g for 20 min at 4℃. The supernatant was collected, and Bradford assays were used to measure the protein concentrations. Equal protein amounts (20 μg) were separated by 10% (W/V) sodium dodecyl sulfate (SDS) polyacrylamide

gel electrophoresis and then transferred onto 0.45-μm pore size nitrocellulose membrane (Bio-Rad Laboratories, Hercules, CA, USA) for 1 hr at 100 V. After 1 hr of blocking in 5% skim milk dissolved in 0.1% Tween-20 containing Tris-buffered saline (TBST) at pH 7.4 for 1 hr at room temperature, the membranes were incubated overnight at 4℃ with primary antibodies against p-p38 (1:1000), p-JNK (1:1000), p-ERK (1:2000), p-IκBα (1:2000), p38 (1:2000), JNK (1:2000), ERK (1:2000), IκBα (1:2000), iNOS (1:1000) and actin (1:2000). After washing with TBST three times for 10 min each, the membrane was incubated with goat anti-rabbit IgG-horseradish peroxidase (HRP) or anti-mouse IgG-HRP for 1 hr and then rinsed three times with TBST. The blot was immunolabeled with enhanced chemiluminescence HRP substrate (Thermo Fisher Scientific Inc., Rockford, IL, USA), and a ChemiDoc™ XRS plus (Bio-Rad laboratories, Hercules, CA, USA) was used to analyze the immunoblot. Actin was used as the loading control for the total protein.

Immunocytochemistry

To confirm the NF-κB activation induced by TMT, the translocation of the NF-κB p65 subunit was observed via an immunocytochemistry method. Additionally, CD11b immunofluorescence was detected to examine the differences in expression between the different groups. CD11b is a cell surface molecule of microglia that is increased in the activated microglia and has been widely used as a marker in microglial activation (Liu et al. 2011; Wakselman et al. 2008). Briefly, 1.5

x 10^4 cells were seeded on poly-L-lysine-coated glass coverslips. After 12 hr of TMT treatment, fixation with 4% paraformaldehyde was performed at room temperature for 15 min. The coverslips were washed three times with PBS and blocked with PBS containing 3% BSA, 0.3% Triton X-100 and 10% NGS for 1 hr. Next, the cells were stained overnight with the following primary antibodies: rabbit polyclonal NF-κB p65 (1:100) (Santa Cruz) and rat polyclonal CD11b (1:100) (AbD Serotec). Following three washes with PBS, the coverslips were incubated with fluorescein isothiocyanate (FITC)-conjugated goat anti-rabbit or donkey anti-rat IgG antibody (1:200) for 1 hr. Hoechst 33258 was added to the slides 15 min prior to finishing the incubation with the secondary antibody. After three additional rinses, the coverslips were placed on the glass slides with an anti-fading mounting medium (Invitrogen, Carlsbad, CA, USA). Immunofluorescence images were obtained from a fluorescence microscope (Axioskop 40; Carl Zeiss, Jena, Germany) at 40x magnification.

Measurement of NO and TNF-α release in the culture medium

In a 24-well tissue culture plate (Thermo Fisher Scientific Inc.), 2.5 x 10^4 cells were seeded in low-glucose DMEM with 1% (v/v) FBS for 24 hr. After 24 hr, the medium was transferred and centrifuged at 500 g for 5 min at 4℃. The supernatant fraction was collected for use in the measurements of NO and TNF-α. For the NO measurements, a general protocol that has been described previously was followed (Wilms et al. 2003). Briefly, 90 μL of each sample and 10 μL of Griess reagent

(containing 0.1% N-[1-naphthyl] ethylenediamine dihydrochloride in 5% H_3PO_4 with 1% of sulfanilic acid) were placed in 96-well tissue culture plate (BD Biosciences). For the standard values, different concentrations of sodium nitrite solution and Griess reagent were placed into the plate. The plate was then gently shaken for 30 min. Absorbance was read in a microplate reader at 540 nm. The nitrite concentration of each sample was calculated from the standard curve. To measure the amount of released TNF-α, a TNF-α enzyme-linked immunosorbent assay (ELISA) kit was obtained from Abcam (Cambridge, UK). Each dilution of the standard and each sample were placed in the plate, and subsequent experiments were performed according to manufacturer's protocol. The TNF-α measurements were collected using a microplate reader at 450 nm. The concentration of each sample was calculated from the standard curve.

Co-culture with HT22 cells using a transwell insert and cell death determination

Propidium iodide (PI) fluorescence was measured with a microplate reader (Nieminen et al. 1992) for the cytotoxicity assay. In a 24-well tissue culture plate, 5.0 x 10^4 cells were seeded per well. An insert with a pore size of 0.4 μm (Millipore, Cat #PICM 012 50) was placed into each well of the culture plate, and 2.5 x 10^4 BV-2 cells were seeded on the insert. Both cell types were adequately submerged in the culture medium that contained high-glucose DMEM with 10% (v/v) FBS. After overnight incubation at 36℃ in a 5% CO_2

incubator, the medium was replaced with low-glucose DMEM with 1% FBS without antibiotics. The inhibitors or vehicle pre-treatments were applied to the BV-2 cells 1 hr before, and the TMT treatment was the applied for 24 hr. Once the treatments were completed, the inserts were removed. Next, PI (final concentration, 20 μg/ml) was added to the wells, which were then incubated at 36℃ in 5% CO_2 for 30 min. The fluorescence was measured by a microplate reader at an excitation at 530 nm, with emission at 630 nm. After measuring the fluorescence of each sample, cell lysis buffer was added to each well to address the total amount of PI fluorescence. Percentage of cell death of each sample was calculated as [fluorescence of treated cells /fluorescence of lysed cells] x 100.

Statistical analyses

The data are presented as mean ± SEM. GraphPad Prism version 5.0 (San Diego, CA, USA) for Windows was used to analyze the data. The one-way analyses of variance (ANOVAs) with Tukey's multiple comparision test was used to examine the differences between groups. A p-value below 0.05 was considered to be statistically significant.

Results

TMT stimulated intracellular ROS generation in BV-2 cells

The BV-2 cells were incubated with various concentrations (300 nM - 5 μM) of TMT for 24 hr, and cell viabilities were then evaluated with MTT assays. As shown in Fig. 1a, 300 nM - 3 μM TMT did not significantly affect cell viability. The cell viability was 92.9 ± 5.1% at 3 μM TMT, which was decreased to 81.1 ± 2.7% at 5 μM TMT compared with the control group. For further investigations, 3 μM TMT was chosen to rule out the significant cell death induced by TMT.

Oxidative stress is generally proposed to contribute on the primary events of cytotoxicity that are caused by various compounds (Eskes et al. 2003; Lull and Block 2010). Previous studies have shown that TMT triggers oxidative burden in both the CNS and several cell lines (Gunasekar et al. 2001; Wang et al. 2008; Qing et al. 2013). We initially determined whether the toxin stimulated ROS production in BV-2 cells. Following the TMT exposure, DCFH-DA staining was performed and quantified by flow cytometry at each indicated time. Increases in ROS generation were detected within 1 hr of the TMT treatment (Fig. 1b). A sustained increase in DCF-fluorescence was observed up to 6 hr and reached 1.85-fold that of the control (Fig. 1b). As ROS production in phagocytes, such as microglia, is predominantly caused by NADPH oxidase distributed on the cell surface that senses the stimuli (Wakselman et al. 2008), we next examined whether NADPH

oxidase might be involved in TMT-induced ROS generation in BV-2 cells. To inhibit the enzyme activity, 250 μM of apocynin was applied 1 hr prior to TMT treatment. Consequently, the intracellular ROS induced by TMT at 6 hr was markedly diminished (Fig. 1c). These data suggest that NADPH oxidase might play a crucial role in the production of oxidative stress in TMT-treated BV2 cells.

TMT activated p38 and JNK MAPK in BV-2 cells

The involvement of MAPK activations in TMT-induced neurotoxicity has been previously reported in both the murine hippocampus (Ogita et al. 2004) and neuroblastoma cells (Jenkins and Barone 2004; Qing et al. 2013). We examined whether TMT could activate MAPK signaling cascades in BV-2 cells. The treated cells were then subjected to western blot analyses at each of the indicated time points. As shown in Fig. 2, TMT led significant increases in p-JNK at 2, 4 and 6 hr after TMT treatment (Fig. 2a). p-p38 also gradually increased from 4 hr to 8 hr of TMT treatment (Fig. 2b). However, the TMT-induced p-ERK exhibited transient changes throughout the time course and decreased at 8 hr after TMT treatment (Fig. 2c).

TMT exposure activated NF-κB signaling in BV-2 cells

In activated microglia, NF-κB signaling is considered to participate in inflammatory processes that result in the expression of inflammatory mediators, including iNOS and some cytokines, such as TNF-α and IL-1β (Lull and Block 2010). NF-κB-dependent mechanism studies have been performed in

BV-2 cells via stimulation with LPS (Liu et al. 2011; Xing et al. 2011), rotenone (Gao et al. 2013) and Aβ (Bachstetter et al. 2011; He et al. 2011) to induce inflammatory processes; however, it has not yet been reported whether TMT regulates NF-κB activation in BV-2 cells. We further determined the alternations of NF-κB signaling that followed exposure to TMT. Because IκBα is known to be an inhibitory subunit of the NF-κB complex that prevents the nuclear translocation of NF-κB, the expression levels of IκBα and phospho-IκBα protein were analyzed by western blot. Consequently, progressive trends of IκBα degradation and p-IκBα elevation were detected over time (Fig. 3). Typically, at 6 and 12 hr post-TMT treatment, IκBα phosphorylation and the degradation of IκBα were most apparent (Fig. 3a,b); these findings indicate that the TMT induced NF-κB activation in BV-2 cells. Next, to examine the involvement of MAPKs on TMT-induced NF-κB activation, SB203580 (p38 MAPK inhibitor), SP600125 (JNK MAPK inhibitor) and BAY11-7082 (IκBα phosphorylation inhibitor) were applied prior to TMT treatment. As shown in Fig. 4a, western blot analyses revealed that TMT significantly elevated p-IκBα expression and that its expression was suppressed by treatment with BAY11-7082. In the same experimental conditions, SB203580 and SP600125 also reduced the TMT-induced elevation of p-IκBα. Furthermore, the translocation of the NF-κB p65 subunit into the nucleus was determined after 12 hr of TMT treatment by immunocytochemistry (Fig. 4b). As shown in Fig. 4b, the NF-κB p65 subunits were localized in the cytosol in the controls

(Fig. 4b-1); however, once the cells were stimulated with TMT, the subunits translocated from the cytosol into the nucleus (Fig. 4b-2). However, pretreatment with SB203580 (Fig. 4b-3) or SP600125 (Fig. 4b-4) inhibited the nuclear translocation of the NF-κB p65 subunits that was induced by TMT treatment. These data suggest that the activation of NF-κB was regulated by MAPKs, particularly p38 and JNK, in the TMT-treated BV-2 cells.

p38 and JNK activations occur earlier than NF-κB activation in TMT-treated BV-2 cells

According to the data shown in Fig. 4, upon TMT exposure, NF-κB activation by p38 and JNK was confirmed by comparing the alterations in p-IκBα and NF-κB p65 nuclear translocation. The regulation of TMT-induced MAPK activation was then examined using BAY11-7082. Consequently, the levels of p-p38 and p-JNK were not affected by BAY11-7082, but each MAPK inhibitor (i.e., SB203580 and SP600125) markedly blocked its expression at 6 hr post-TMT treatment (Fig. 5a, b). These data suggest that MAPK activation is upstream of the NF-κB pathway. Together, these findings suggest that the TMT-induced p38 and JNK activations occurred prior to NF-κB activation in BV-2 cells.

TMT induced increases in iNOS expression and the production of NO and TNF-α in BV-2 cells

The levels of some proinflammatory molecules, such as NO and TNF-α, were then examined in the culture media after the

TMT treatments of the BV-2 cells because these factors have been reported to participate with NF-κB activation in the responses to various stimuli (Lull and Block 2010; Ransohoff and Perr 2009; Wakselman et al. 2008). First, we examined iNOS expression at 12 hr by western blot analysis (Fig. 6a). TMT significantly increased iNOS expression by approximately 2.5-fold compared to the control; however, this effect was reversed by pretreatment with SB203580, SP600125 or BAY11-7082. Next, the amounts of released NO at 24 hr were quantified using the Griess reagent method (Fig. 6b). TMT treatment elevated NO production by approximately 6-fold compared to that observed in the control (control; 0.28 ± 0.16 μM, TMT; 1.67 ± 0.18 μM). Pretreatment with SB203580 reduced the TMT-stimulated NO production by approximately 53%, from 1.67 ± 0.18 μM to 0.79 ± 0.24 μM. SP600125 and BAY11-7082 were also attenuated the TMT-induced NO level to 0.31 ± 0.17 μM and 0.58 ± 0.29 μM, respectively. Moreover, TNF-α secretion from the treated BV-2 cells was determined at 24 hr in an ELISA. Continuous TNF-α secretion resulted from TMT-treatment and reached 53-fold the control level. However, the massive increase in TNF-α from TMT treatment was significantly reversed by pretreatment with SB203580, SP600125 or BAY11-7082 (Fig. 6c).

CD11b expression was increased in the TMT-treated BV-2 cells

CD11b and other microglial markers, including CD11a, CD11c, CD18, and others, have been reported to prominently appear in

many neurodegenerative diseases (Roy et al. 2006). Hence, we visualized the activated microglial cells with CD11b immunostaining at 12 hr post-TMT treatment. As Fig. 7-1 shows, a faint cytoplasmic staining for CD11b can be observed in the control. Following TMT treatment (Fig. 7-2), green fluorescence was detected more intensively compared to Fig. 7-1, 7-3 and 7-4, indicating that SB203580 and SP600125 prevented the elevation of CD11b expression that resulted from TMT treatment. These results support the notion that TMT elicited microglial activation by increasing CD11b surface molecules in BV-2 cells and that the p38 and JNK MAPK activations induced by TMT contributed to this increase in CD11b expression.

The NADPH oxidase inhibitor apocynin prevented the TMT-induced activations of MAPKs and NF-κB in the BV-2 cells

Our observations revealed that NADPH oxidase-dependent ROS generation occurred in BV-2 cells and that treatment with apocynin remarkably suppressed the TMT-induced oxidative stress. Therefore, we further investigated the role of toxin-induced ROS generation on microglial activation. Importantly, reductions in NADPH oxidase activity mediated by apocynin treatment significantly decreased TMT-induced p-p38 and p-JNK (Fig. 8a, b)although apocynin itself was able to reduce p-p38 compared to control (Fig. 8a) at 6 hr post-TMT treatment. Moreover, apocynin inhibited TMT-induced NF-κB activation and iNOS expression as shown by the western blot analyses of p-IκBα and iNOS at 12 hr (Fig. 8c, d), and consequently

reduced release of TMT-induced NO (approximately 70%) and TNF-α (approximately 94%) after 24 hr of TMT treatment (Fig. 8e.f). Thus, these data suggest that NADPH oxidase activity was the major source of TMT-induced ROS generation and that intracellular ROS signaling is an upstream effector in BV-2 microglial activation.

TMT-activated microglia evoked cell death in HT22 cells

The following experiment was designed to further explore the role of TMT-induced microglial activation on neuronal cell survival. HT22 neuronal cells were seeded on culture plate, and inserts containing BV-2 cells were fitted into the wells. To avoid HT22 cell death during the experiment, 1% (v/v) of FBS was given during the test, and any inhibitors were applied to the BV-2 cells on the insert. After 24 hr, the inserts were removed, and cell death of the HT22 cells was examined by the cytotoxicity assay. Interestingly, treatment with 3 μM TMT led to neuronal cell death at a rate that exceeded that observed in the controls by 3.75-fold (control; 7.63 $\pm$ 0.42%, TMT; 24.33 $\pm$ 0.33%) (Fig. 9). The rates of cell death that resulted from pre-treatment with SB203580, SP600125 and apocynin were 14.75 $\pm$ 0.61 %, 8.91 $\pm$ 1.65 % and 8.28 $\pm$ 2.66 %, respectively, and these treatments effectively prevented TMT-induced neuronal cell death (Fig. 9). The direct exposure of the HT22 cells to 3 μM TMT, without the BV-2 cells, did not affect neuronal cell death (data not shown).

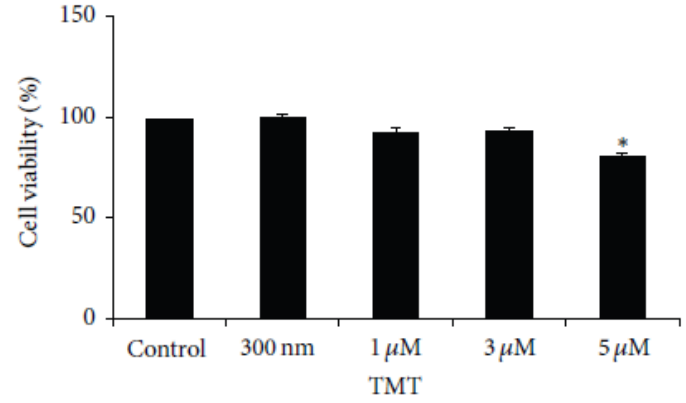
150
100
50
0
Cell viability (%)
*
Control
300 nm
1 μM
3 μM
5 μM
TMT

(a)

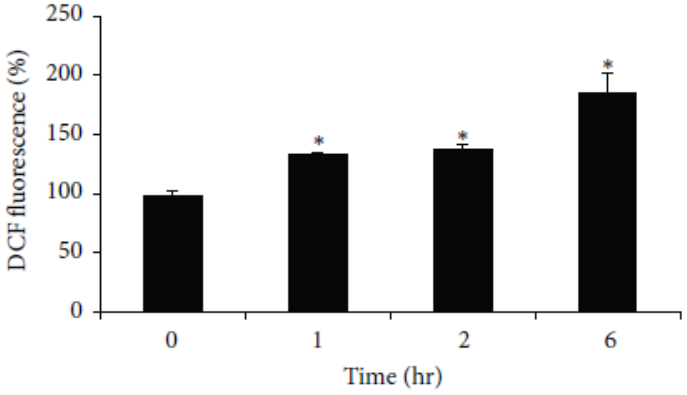
250
200
150
100
50
0
DCF fluorescence (%)
*
*
*
0
1
2
6
Time (hr)

(b)

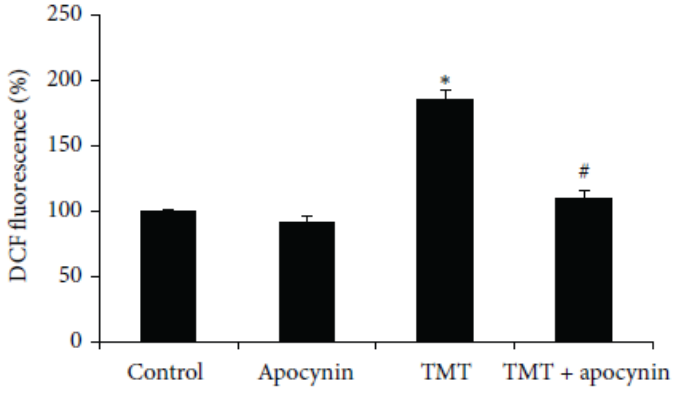
250
200
150
100
50
0
DCF fluorescence (%)
*
#
Control
Apocynin
TMT
TMT + apocynin

(c)

Fig. 1 TMT-stimulated ROS generation in BV-2 cells. (a) For the cell viability test, the cells were treated with various concentrations of TMT (300 nM - 5 μM) or vehicle (saline) for 24 hr, then MTT assay was performed to measure the cell viability. The value of each sample was normalized to control group. (b) For ROS measurement, 3 μM TMT treated cells were incubated for the indicated periods of time (0 - 6 hr) and then, stained with 15 μM DCFH-DA for 30 min. DCF-fluorescence of each sample was analyzed by the flow cytometry. The value measured at 0 hr was set as 100 %. The data are represented as mean ± SEM (n = 4). $*P < 0.05$ compared with control (0 hr). (c) Cells were pre-treated with 250 μM apocynin prior to TMT treatment and then incubated for 6 hr. The data are represented as mean ± SEM (n = 4). $*P < 0.05$ compared with the value of control, $^{\#}P < 0.05$ compared with the value of TMT

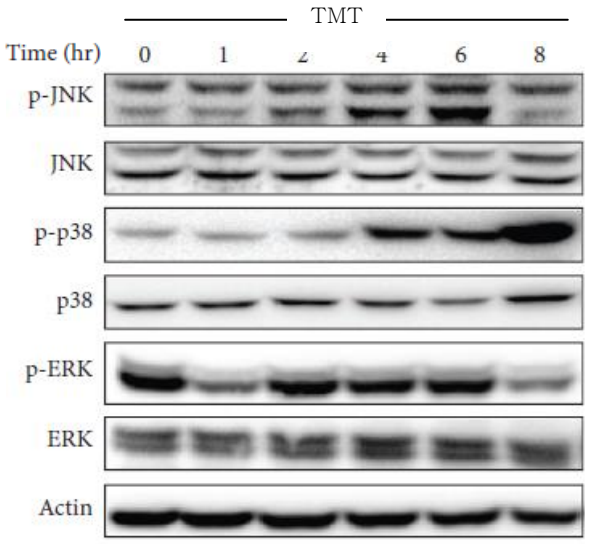
TMT
Time (hr) 0 1 2 4 6 8
p-JNK
JNK
p-p38
p38
p-ERK
ERK
Actin

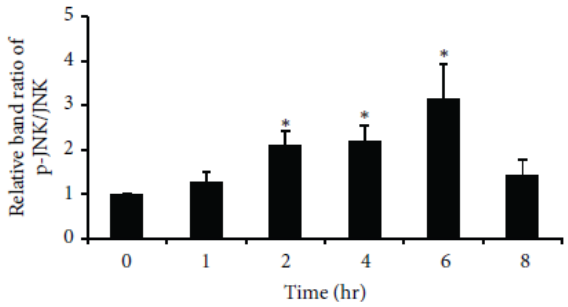
Relative band ratio of p-JNK/JNK
0 1 2 3 4 5
0 1 2 4 6 8
Time (hr)

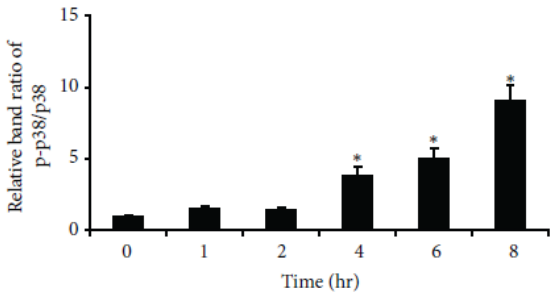
Relative band ratio of p-p38/p38
0 5 10 15
0 1 2 4 6 8
Time (hr)

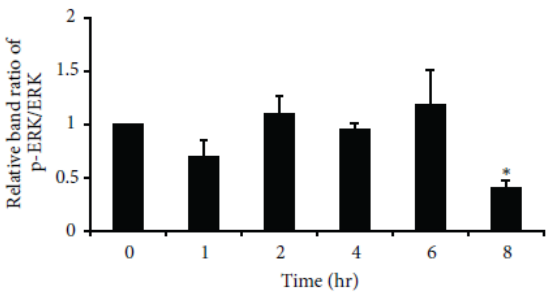
Relative band ratio of p-ERK/ERK
0 0.5 1 1.5 2
0 1 2 4 6 8
Time (hr)

Fig. 2 p38 and JNK were activated by TMT exposure in BV-2 cells. Treated cells were analyzed by western blot at each time period. The bar graphs represent the band intensity of each phospho-form of MAPKs normalized to total. The data are represented as mean ± SEM (n = 5). $*P < 0.05$ compared with the control group

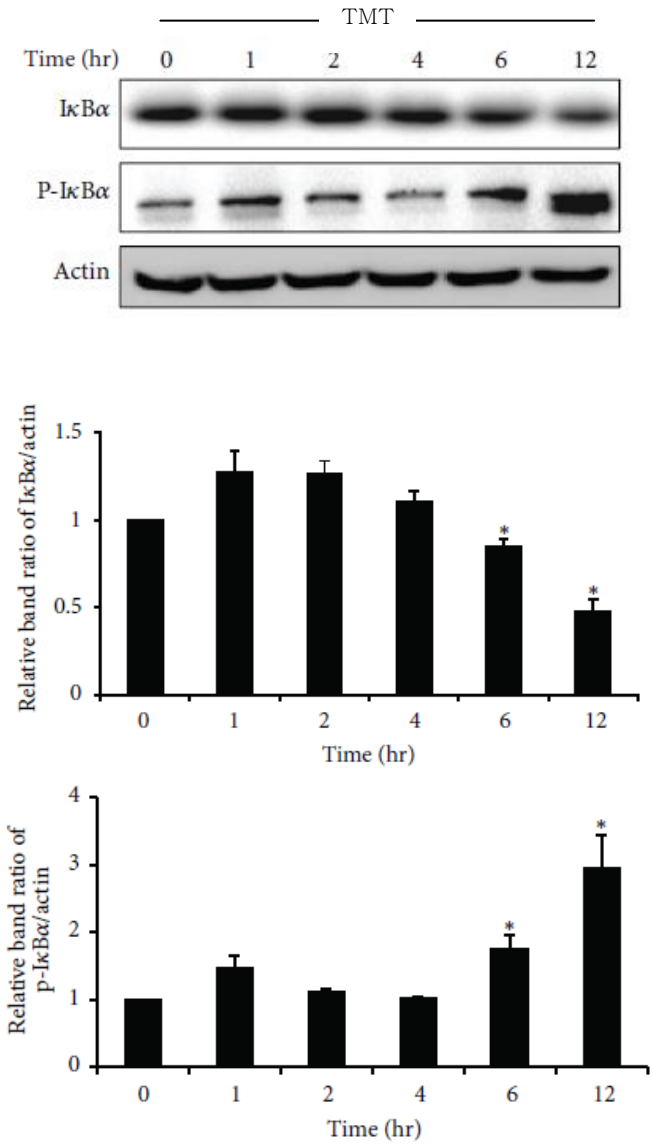

Fig. 3 NF−κB signaling pathway was activated by TMT exposure in BV−2 cells. Treated cells were subjected to western blot analysis. The bar graphs represent the band intensity of each protein normalized to actin. The data are represented as mean ± SEM (n = 5). $*P < 0.05$ compared with the control group

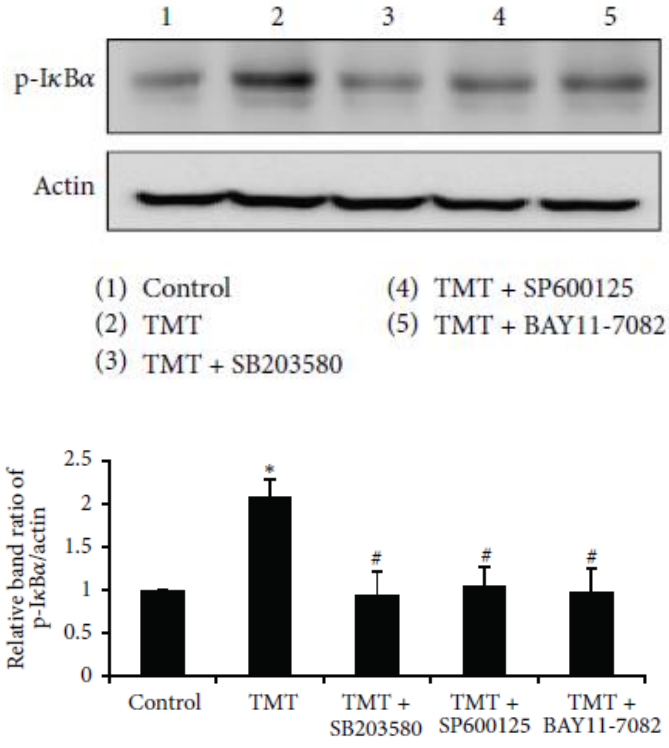
1
2
3
4
5
p-IκBα
Actin
(1) Control
(2) TMT
(3) TMT + SB203580
(4) TMT + SP600125
(5) TMT + BAY11-7082
Relative band ratio of p-IκBα/actin
2.5
2
1.5
1
0.5
0
*
#
#
#
Control
TMT
TMT + SB203580
TMT + SP600125
TMT + BAY11-7082

(a)

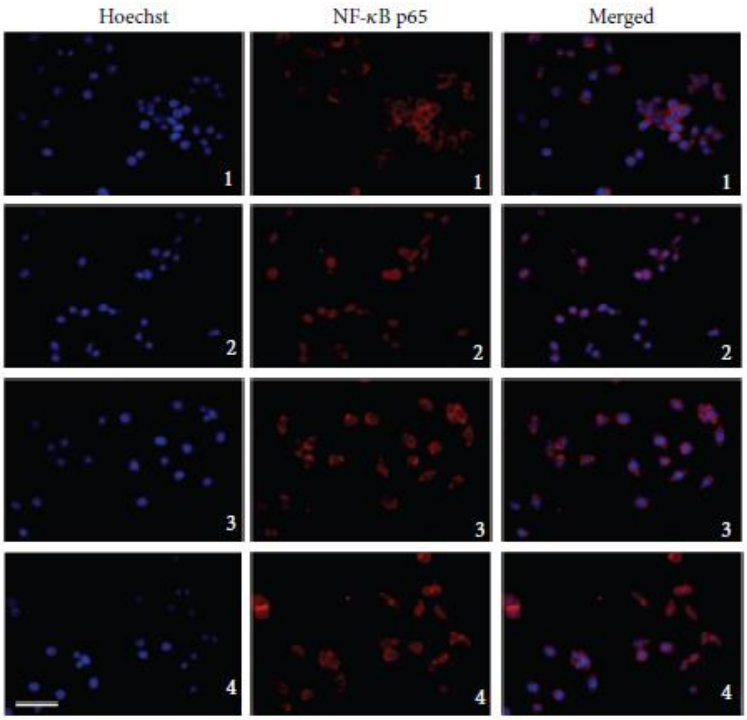

(b)

Fig. 4 TMT-induced NF-κB activation was reversed by p38 and JNK inhibitor in BV-2 cells. SB203580, SP600125 and BAY11-7082 were pre-treated for 1 hr and incubated with TMT for 12 hr. (a) Protein expression of phospho-IκBα was shown by western blot. The bar graph represents the band intensity of phospho-form normalized to actin. The data are represented as mean ± SEM (n = 5). $*P < 0.05$ compared with the control group. (b) Following the fixation of treated cells, immunocytochemistry method was carried to observe the translocation of NF-κB p65 subunit morphologically. NF-κB p65 subunit was detected by red fluorescence (Alexa 568), nucei were stained with blue fluorescence (Hoechest 33258) and the two different types of images were merged. The experiments were repeated more than 3 times.
1: control, 2: TMT, 3: TMT+SB203580, 4: TMT+SP600125, 5: TMT+BAY11-7082

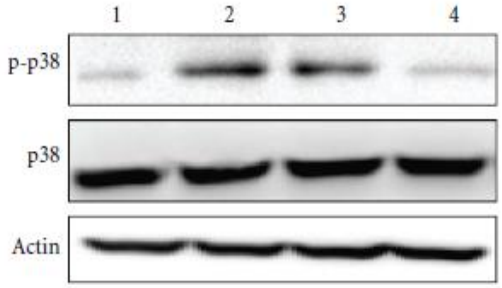

(1) Control
(2) TMT
(3) TMT + BAY11-7082
(4) TMT + SB203580

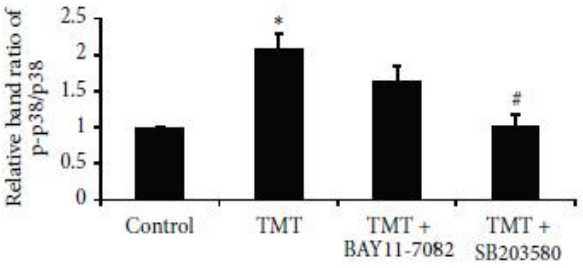

(a)

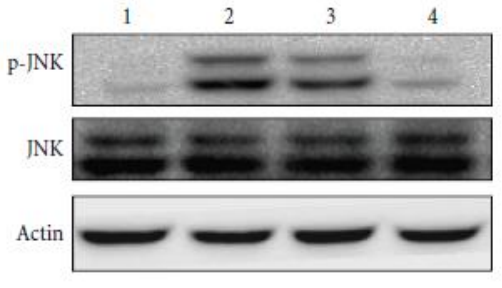

(1) Control
(2) TMT
(3) TMT + BAY11-7082
(4) TMT + SP600125

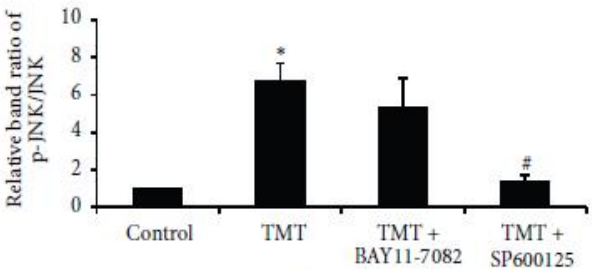

(b)

Fig. 5 p38 and JNK phosphorylation were followed by NF-κB activation upon the TMT exposure in BV-2 cells. Treated cells were collected at 6 hr and were subjected to western blot analysis. The bar graphs represent the band intensity of each phospho-form normalized to total. The data are represented as mean ± SEM (n = 5). *P < 0.05 compared with the control group, #P < 0.05 compared with the value of TMT

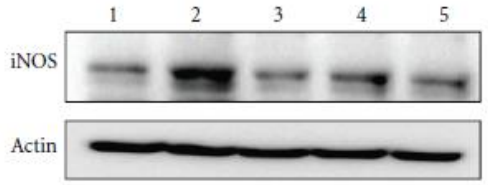

(1) Control
(2) TMT
(3) TMT + SB203580
(4) TMT + SP600125
(5) TMT + BAY11-7082

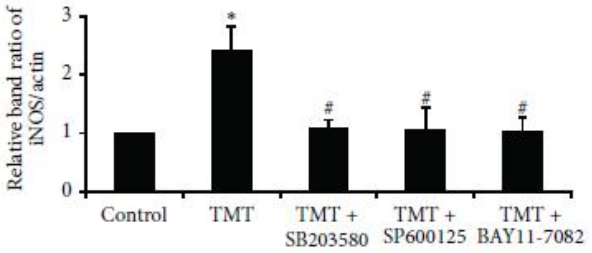

(a)

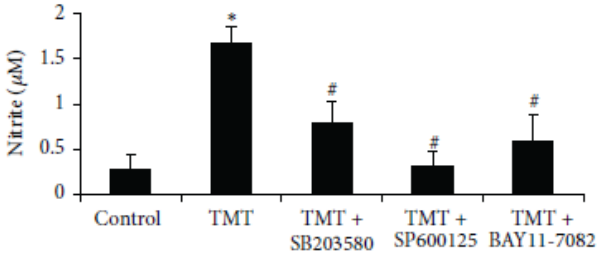

(b)

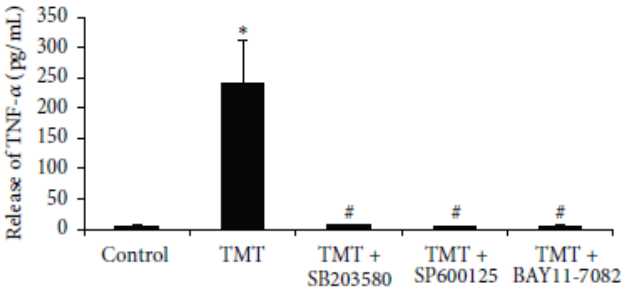

(c)

Fig. 6 TMT increased iNOS expression and the production of NO and TNF-α in BV-2 cells. (a) At 12 hr, the expression of iNOS was analyzed by western blot. The bar graphs represent the band intensity of each protein normalized to actin. (b) At 24 hr, the culture media was taken to access the level of NO by Griess method. (c) The culture media were also transferred into TNF-α Elisa kit to measure the level of TNF-α released from the treated cells. The concentration of TNF-α (pg/ml) was measured by standard curve. The data are represented as mean $\pm$ SEM (n = 5 - 7). $*P < 0.05$ compared with the control group, $^{\#}P < 0.05$ compared with the value of TMT.
1: control, 2: TMT, 3: TMT+SB203580, 4: TMT+SP600125,
5: TMT+BAY11-7082

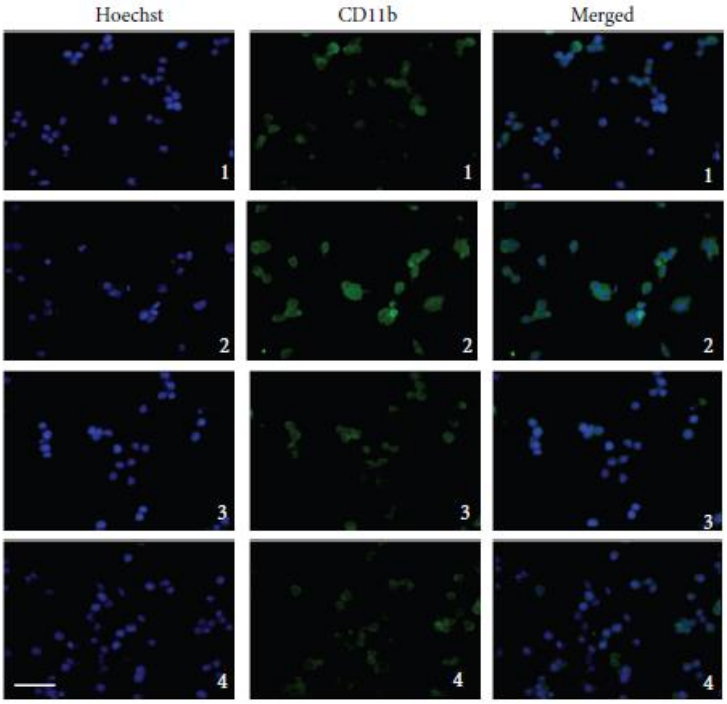

Fig. 7 TMT enhanced the expression of CD11b in BV-2 cells. The cells were treated and after 12 hr, immunocytochemistry was carried to observe the change of CD11b expression among different groups. CD11b was detected by green fluorescence (Alexa 488) and nuclei were stained with blue fluorescence (Hoechst 33258). The two different types of images were merged. The experiments were repeated more than 3 times
1: control, 2: TMT, 3: TMT+SB203580, 4: TMT+SP600125

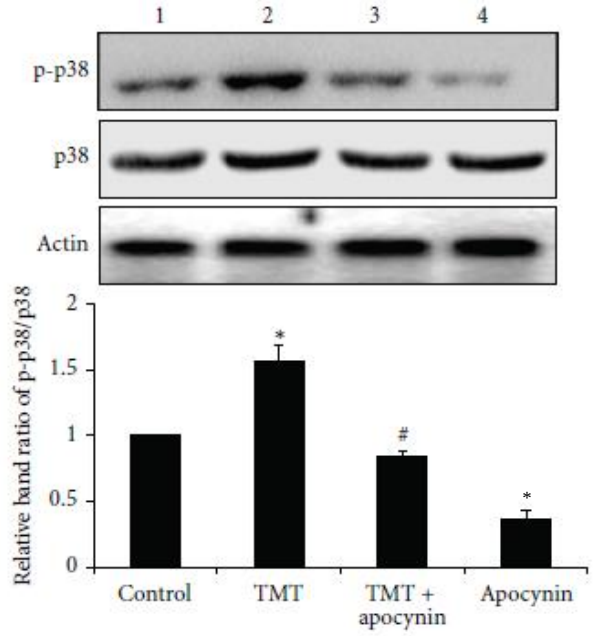
1
2
3
4
p-p38
p38
Actin
Relative band ratio of p-p38/p38
2
1.5
1
0.5
0
*
#
*
Control
TMT
TMT + apocynin
Apocynin

(a)

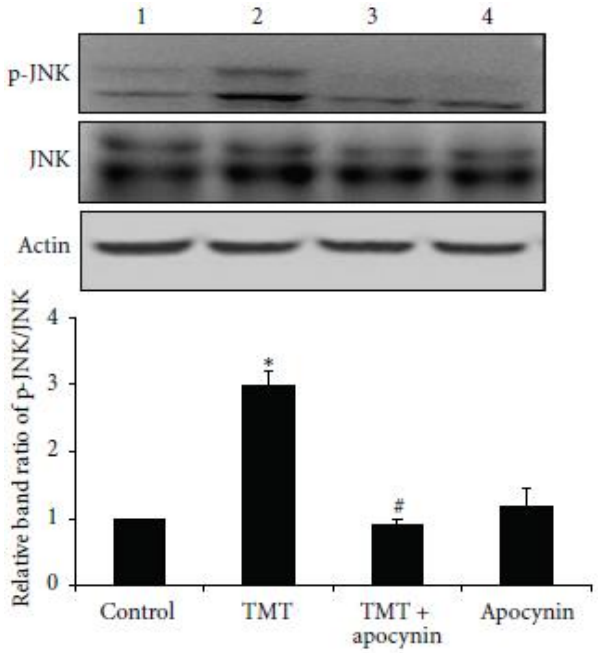
1
2
3
4
p-JNK
JNK
Actin
Relative band ratio of p-JNK/JNK
4
3
2
1
0
*
#
Control
TMT
TMT + apocynin
Apocynin

(b)

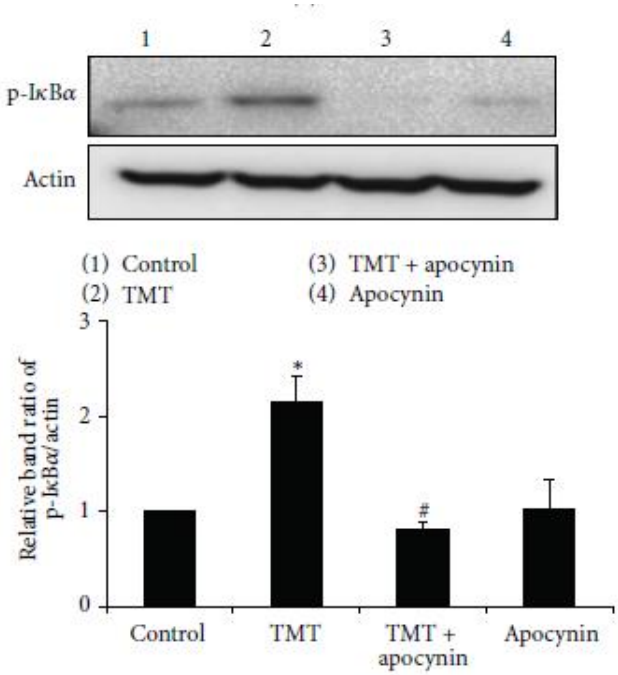
1
2
3
4
p-IκBα
Actin
(1) Control
(2) TMT
(3) TMT + apocynin
(4) Apocynin
Relative band ratio of p-IκBα/actin
3
2
1
0
*
#
Control
TMT
TMT + apocynin
Apocynin

(c)

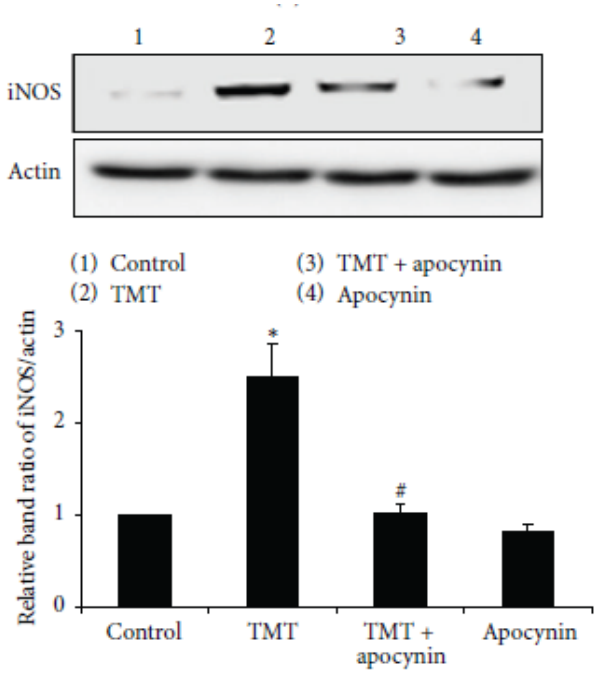
1
2
3
4
iNOS
Actin
(1) Control
(2) TMT
(3) TMT + apocynin
(4) Apocynin
Relative band ratio of iNOS/actin
3
2
1
0
*
#
Control
TMT
TMT + apocynin
Apocynin

(d)

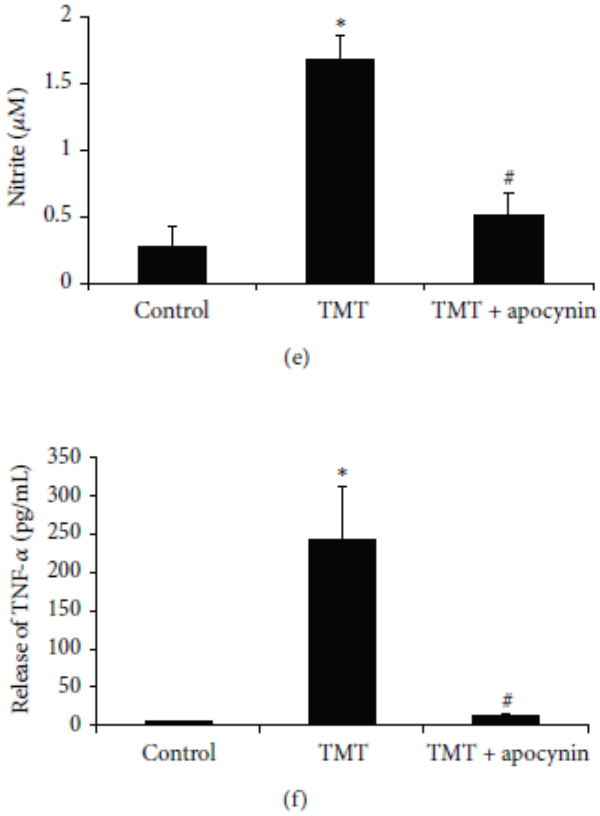

Fig. 8 Apocynin suppressed TMT−induced MAPKs activations, p−IKB, iNOS, NO production and TNF−α release in BV−2 cells. (a)−(d) the treated cells were subjected to western blot analysis to access the expression of phosphorylated p38 and JNK at 6 hr, p−IκBα and iNOS at 12 hr. The bar graphs represent the band intensity of each protein form normalized to total. For (e) and (f), the culture media of treated cells at 24 hr were collected and used for (e) NO production measurement by Griess reagent method and (f) TNF−α detection by using Elisa kit. The data are represented as mean ± SEM (n = 4 − 7) $*P < 0.05$ compared with the control group, $^{\#}P < 0.05$ compared with the value of TMT.
1: control, 2: TMT, 3: TMT+Apocynin, 4: Apocynin

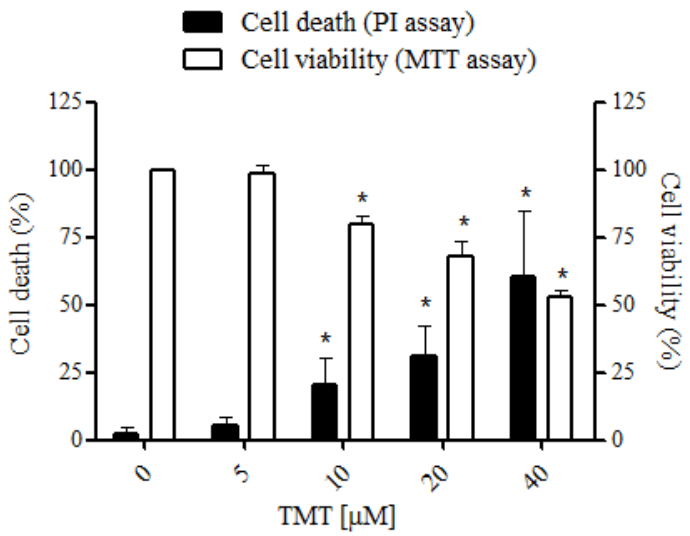
Cell death (PI assay)
Cell viability (MTT assay)
Cell death (%)
Cell viability (%)
125
100
75
50
25
0
0
5
10
20
40
TMT [μM]
*

(a)

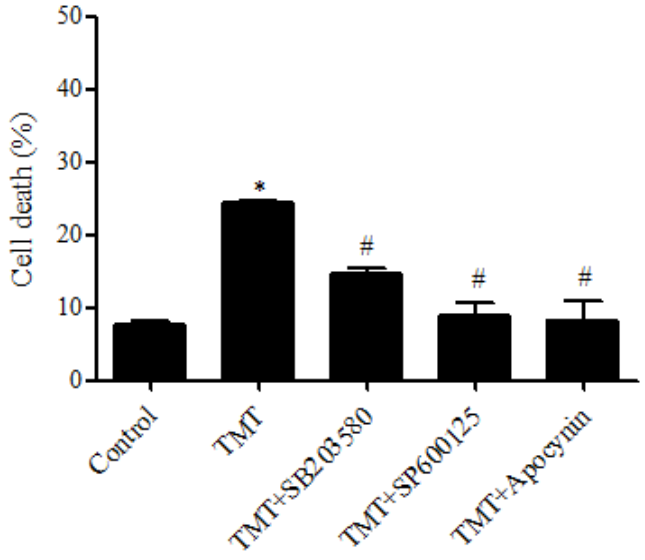
Cell death (%)
50
40
30
20
10
0
*
#
Control
TMT
TMT+SB203580
TMT+SP600125
TMT+Apocynin

(b)

Fig. 9 TMT-activated BV-2 cells rendered HT22 neuronal cell death. (a) HT22 cells were seeded on 24-well culture plate without insert and then treated with various concentrations of TMT (5 μM - 40 μM) for 24 hr, then cell death was determined by PI and MTT assays. (b) HT22 cells were seeded on the cell culture plate and BV-2 cells were seeded on the trans-well insert. Different inhibitors; SB203580, SP600125 and apocynin were treated onto the microglial cells prior to the administration of 3 μM TMT. In 24 hr, HT22 cells were analysed by PI assay to account the cell death. The data are represented as mean ± SEM (more than 4 times). $*P < 0.05$ compared with the control group, $^{\#}P < 0.05$ compared with the value of TMT

Discussion

The purpose of this study was to investigate whether TMT can directly activate BV-2 microglia cells and, if so, to identify the signaling pathways that are involved in its activation. Our present observations revealed that TMT initially induced robust intracellular ROS generation that was followed by p38 and JNK activation. Subsequently, NF-κB was activated, resulting in NO and TNF-α production in the BV-2 cells. In a co-culture system of BV-2 and HT22 cells, neuronal cell death was induced by TMT treatment of the microglia. These results indicate that BV-2 cells can be directly activated by TMT to generate an oxidative burden and pro-inflammatory mediators, such as NO and TNF-α; these soluble factors participate in neuronal cell death.

Microglia are the innate immune cells of the CNS and play a crucial role in host defense against various invaders (Wakselman et al. 2008). In response to various stimuli, microglia can be activated, which can include the following changes: 1) their morphologies can become ramified, amoeboid, or phagocytic (Eskes et al. 2003; Ransohoff and Perry 2009); 2) expression of cell surface antigens, including CD11b, Iba-1, and OX-42 (Wakselman et al. 2008; Yan et al. 2013); and 3) production of bioactive factors, such as NO, O_2^-, prostaglandins (PGs), TNF-α, IL-1, IL-12, and IFN-γ (Lull and Block 2010; Ransohoff and Perry 2009). In the present study, we initially determined whether TMT could directly activate BV-2

cells. We observed increased production of NO, and TNF-α was detected as previously reported by other researchers (Eskes et al. 2003; Noraberg et al. 1998; McPherson et al. 2011). Based on these findings, it can be assumed that TMT activates BV-2 microglial cells. Additionally, we monitored the expression of CD11b, which is a cell surface molecule, to confirm microglial activation following TMT exposure (Liu et al. 2011). Although CD11b can be observed in resting states, its expression is increased after the cells become stimulated (Wakselman et al. 2008). Following TMT treatment, we observed increased CD11b immunocytofluorescence in BV-2 cells, which indicated that TMT activated the BV-2 cells.

How TMT activates microglia to result pro-inflammatory effects in the CNS has remained unclear due to the limited numbers of mechanistic investigations that have been performed. For the first time, in the present study, we examined the direct activation of BV-2 cells by TMT exposure to evaluate the underlying signaling pathways. In *in vitro* studies, some typical observations, such as increased TNF-α release and iNOS over-expression, provided evidence of the TMT-induced activation of primary microglial cells (Eskes et al. 2003; Reali et al. 2005); in contrast, no direct microglial activation has been reported (Röhl and Sievers 2005; Röhl et al. 2009). A few studies have documented that the discrepancies between *in vitro* studies using primary microglia-enriched cultures might have resulted from variations in the resting states of the microglia that depend on the cell isolation and

culture maintenance conditions (Heppner et al. 1998; Ransohoff and Perry 2009; Caldeira et al. 2014). Additionally, BV-2 cells are frequently used as a substitute for primary microglia. It has been reported that approximately 90% of the genes of mouse primary microglial and BV-2 cells overlap following LPS treatment and that this cell line is partially activated in resting states (Henn et al. 2009; Stansley et al. 2012). Based on these reasons, it might be beneficial to analyze microglial activation more clearly during TMT toxicity via the use of BV-2 cells rather than other experimental models (Röhl and Sievers 2005; Röhl et al. 2009).

To evaluate the cellular mechanisms involved in the TMT-induced microglial activation, we performed investigations of the NF-κB and MAPKs signaling pathways, which previously been discussed in numerous studies as upstream effectors that target the production of inflammatory factors in microglia (Lull and Block 2010; He et al. 2011). In the context of TMT, NF-κB activation has been reported in the murine hippocampus (Kassed et al. 2004), human primary astrocytes (Reali et al. 2005) and a human neuroblastoma cell line (Qing et al. 2013). Similarly, in our experiment, NF-κB was activated with evidence of reduced IκBα, increased p-IκBα and nuclear translocation of the NF-κB p65 subunit. Targeting NF-κB activation with BAY11-7082 (a IκBα phosphorylation inhibitor) resulted in remarkable decreases in NO and TNF-α levels. These findings are consistent with those of a previous study (Kim et al. 2014) that observed increased TNF-α, IL-

1β, IL-6 and iNOS mRNA levels in TMT-treated BV-2 cells and mouse hippocampi (Viviani et al. 1998). Recently, it was also reported that dibutyltin, another organotin compound that causes severe immunotoxicity and developmental toxicity in animals (Jenkins et al 2004; Ema et al 2009), induces increases in iNOS, TNF-α and IL-6 mRNA levels in BV-2 cells (Chantong et al. 2014).

Many inflammatory stimuli, such as LPS (Liu et al. 2011), rotenone (Gao et al. 2013) and Aβ (Bachstetter et al. 2011; Xing et al. 2011), have been reported to stimulate BV-2 cells via MAPK activations that result in the modulation of inflammatory factors. Relying on previously reported information, we examined whether TMT could activate MAPKs in BV-2 cells. TMT induced p38 and JNK activation, and pharmacological inhibitions with the p38 MAPK inhibitor SB203580 and the JNK MAPK inhibitor SP600125 prevented TMT-induced NF-κB activation, as shown by reduced p-IκBα and NF-κB p65 translocation into the nucleus. In contrast, inactivation of NF-κB with BAY11-7082 did not affect the TMT-induced p-p38 or p-JNK levels. Next, to elucidate the role of TMT-induced p38 and JNK activations on the production of inflammatory factors in BV-2 cells, further experiments were performed, and remarkable suppressions of TMT-elevated iNOS, NO and TNF-α levels resulted from pre-treatment with SB203580, SP600125 or BAY11-7082. Similarly, decreased CD11b expression was observed following inhibition of MAPK activities. These results suggest that,

following TMT exposure, MAPK activity occurs upstream of NF-κB activation in BV-2 cells. Our present observations are in agreement with those of previous studies (Bachstetter et al. 2011; Gao et al. 2013; Xing et al. 2011).

For the next step, the ROS generation caused by TMT in BV-2 cells was initially examined because TMT-induced intracellular ROS generation has been frequently proposed to be involved in neurotoxicity (Gunasekar et al. 2001; Jenkins and Barone 2004). The generation of ROS in microglia has been suggested to initiate various signaling pathways that are related to cytotoxic mechanisms, such as NF-κB, MAPKs and PI3K/AKT signaling cascades (Gao et al. 2013; Lull and Block 2010). In our experiment, a rapid increase in DCF-fluorescence was observed within 1 hr of TMT treatment. Because the main route of ROS generation in microglia is known to be mediated through the activity of NADPH oxidase, which is localized on the surfaces of phagocytic cells and is up-regulated in response to various stimuli (Lull and Block 2010; Yan et al. 2013), we inhibited microglial NADPH oxidase with apocynin. Apocynin effectively reversed the elevation in the intracellular ROS induced by TMT. Our results are consistent with those of other reports that have illustrated the involvement of NADPH oxidase in ROS generation in response to multiple stimuli in phagocytic cells. Because NADPH oxidase has been implicated in the generation of oxidative stress in BV-2 cells in response to TMT, we further demonstrated the effects of NADPH oxidase-dependent ROS generation on TMT-induced

microglial activation. Interestingly, in addition to the reduction in ROS formation, apocynin prevented the influence of TMT on all parameters, including TMT-increased phosphorylation of p38, JNK and IκBα, iNOS expression, and NO and TNF-α production. Hence, these findings indicate that TMT-induced MAPKs and NF-κB are targeted by intracellular ROS generation in BV-2 cells. The mechanisms involved in regulation of NADPH oxidase has not been evaluated in this study. However, it was reported the involvement of PKC in phagocyte NADPH oxidase activation (Raad et al. 2009). There are some reports that TMT-increased intracellular calcium resulting in rat hippocampal neurons (Piacentini et al. 2008) and TMT-activated PKC leading to cytotoxicity in PC12 cells (Kane et al. 1998). From these studies, it can be suggested that PKC and intracellular calcium might be involved in NADPH oxidase activation in TMT-treated BV-2 cells.

Based on the data we have obtained, we propose that TMT directly activated microglial cells via a process involving NADPH oxidase-dependent ROS generation and p38, JNK and NF-κB activation. Subsequent increases in the bioactive factors of inflammation, NO and TNF-α, were also observed. However, the role of microglial activation remains controversial because microglia interact with several types of cells in the brain, and a complicated process is turned on by the recruitment of diverse signals from different types of cells related to inflammatory stimulus. For example, some studies have reported that inflammatory stimuli, such as LPS and IFN-

γ, induce microglial activation, which leads to neuronal cell death due to the release of TNF-α, but this process can be rescued by treatment with astrocyte-conditioned media or anti-TNF-α antibodies in rat primary cultures (Rozenfeld et al. 2003; Vincent et al. 1997) and BV-2 cells (He et al. 2002). However, the synergistic effect of TNF-α production has also been established following the exposure of co-cultures of microglia and astrocytes to LPS (Solà et al. 2002; Steelman and Li 2014). Based on this finding, the strength of pro-inflammatory microglia can be regulated via interactions with other cells in the brain; therefore, it was necessary to verify the ultimate effects of activated BV-2 cells on neurons during TMT intoxication. For this experiment, we used a co-culture of BV-2 microglial cells with HT22 neuronal cells. The HT22 cells were physically separated from the insert containing the BV-2 cells, but the neuronal cells were still able to access the soluble factors released by the BV-2 cells during the treatment. Therefore, neuronal cell death occurred with a 3 μM dosage of TMT in the presence of BV-2 cells, while the TMT dosage did not mediate cell death in HT22 cells. In addition to these results, the neuronal cell death was also rescued by p38, JNK or NADPH oxidase inactivation. The data obtained from this co-culture experiment suggest some possibility that microglial activation may be deleterious to neuronal cell survival in TMT intoxication. Similarly, a recent study noted that the neuronal cell death observed was induced by activated BV-2 cells upon LPS exposure (Zhu et al. 2014). Nonetheless, it is still undefined which bioactive factors produced from TMT-treated

BV-2 cells are harmful to the neuronal cell survival. Further investigations are required to interpret the role of microglial activation in terms of cell-to-cell interactions in TMT neurotoxicity.

Taken together, our results indicate that TMT directly activates BV-2 cells via oxidative stress and activation of some signaling pathways. TMT-induced oxidative stress mediated p38 and JNK phosphorylation and NF-κB activation. NO and TNF-α production was also observed. These activated microglial cells induced neuronal cell death in HT22 cells for reasons not yet fully understood. However, all of these results were reversed by the inhibition of NADPH oxidase activity. A conclusion that can be made from the present results is that TMT can directly induce BV-2 cells and that NADPH oxidase-dependent ROS generation would be the initial event of a TMT-stimulated cellular response.

References

Akiyama H, Barger S, Barnum S et al (2000) Inflammation and Alzheimer's disease. Neurobiol Aging 21(3):383-421.

Bachstetter AD, Xing B, de Almeida L et al (2011) Microglial p38α MAPK is a key regulator of proinflammatory cytokine up-regulation induced by toll-like receptor (TLR) ligands or beta-amyloid (Aβ). J Neuroinflammation 6;8:79.

Caldeira C, Oliveira AF, Cunha C et al (2014) Microglia change from a reactive to an age-like phenotype with the time in culture. Front Cell Neurosci 2;8:152.

Chantong B, Kratschmar DV, Lister A, Odermatt A (2014) Dibutyltin promotes oxidative stress and increases inflammatory mediators in BV-2 microglia cells. Toxicol Lett 15;230(2):177-87.

Ema M, Arima A, Fukunishi K et al (2009) Developmental toxicity of dibutyltin dichloride given on three consecutive days during organogenesis in cynomolgus monkeys. Drug Chem Toxicol 32(2):150-7.

Eskes C, Juillerat-Jeanneret L, Leuba G et al (2003) Involvement of microglia-neuron interactions in the tumor necrosis factor-alpha release, microglial activation, and neurodegeneration induced by trimethyltin. J Neurosci Res 15;71(4):583-90.

Figiel I, Dzwonek K (2007) TNFalpha and TNF receptor 1 expression in the mixed neuronal-glial cultures of hippocampal dentate gyrus exposed to glutamate or trimethyltin. Brain Res 2;1131(1):17-28.

Furuhashi K, Ogawa M, Suzuki Y et al (2008) Methylation of dimethyltin in mice and rats. Chem Res Toxicol 21(2):467-71.

Gao F, Chen D, Hu Q, Wang G (2013) Rotenone directly induces BV2 cell activation via the p38 MAPK pathway. PLoS One 20;8(8):e72046. doi: 10.1371/journal.pone.0072046.

Geloso MC, Corvino V, Michetti F (2011) Trimethyltin-induced hippocampal degeneration as a tool to investigate neurodegenerative processes. Neurochem Int.58(7):729-38.

Gunasekar P, Li L, Prabhakaran K et al (2001) Mechanisms of the apoptotic and necrotic actions of trimethyltin in cerebellar granule cells. Toxicol Sci 64(1):83-9.

He BP, Wen W, Strong MJ (2002) Activated microglia (BV-2) facilitation of TNF-alpha-mediated motor neuron death in vitro. J Neuroimmunol 128(1-2):31-8.

He FQ, Qiu BY, Li TK et al (2011) Tetrandrine suppresses amyloid-β-induced inflammatory cytokines by inhibiting NF-κB pathway in murine BV2 microglial cells. Int Immunopharmacol 11(9):1220-5.

Henn A, Lund S, Hedtjärn M et al (2009) The suitability of BV2 cells as alternative model system for primary microglia cultures or for animal experiments examining brain inflammation. ALTEX 26(2):83-94.

Heppner FL, Roth K, Nitsch R, Hailer NP (1998) Vitamin E induces ramification and downregulation of adhesion molecules in cultured microglial cells. Glia 22(2):180-8.

Ishikawa K, Kubo T, Shibanoki S et al (1997) Hippocampal degeneration inducing impairment of learning in rats: model of dementia? Behav Brain Res 83(1-2):39-44.

Ishikura N, Tsunashima K, Watanabe KI et al (2001) Temporal change of hippocampal enkephalin and dynorphin mRNA following trimethyltin intoxication in rats: effect of anticonvulsant. Neurosci Lett 306(3):157-60.

Jenkins SM, Barone S (2004) The neurotoxicant trimethyltin induces apoptosis via caspase activation, p38 protein kinase, and oxidative stress in PC12 cells. Toxicol Lett 28;147(1):63-72.

Jenkins SM, Ehman K, Barone S Jr (2004) Structure-activity comparison of organotin species: dibutyltin is a developmental neurotoxicant in vitro and in vivo. Brain Res Dev Brain Res 19;151(1-2):1-12.

Kane MD, Yang CW, Gunasekar PG et al (1998) Trimethyltin stimulates protein kinase C translocation through receptor-

mediated phospholipase C activation in PC12 cells. J Neurochem 70(2):509-14.

Kassed CA, Butler TL, Patton GW et al (2004) Injury-induced NF-kappaB activation in the hippocampus: implications for neuronal survival. FASEB J 18(6):723-4.

Kim J, Yang M, Son Y et al (2014) Glial activation with concurrent up-regulation of inflammatory mediators in trimethyltin-induced neurotoxicity in mice. Acta Histochem 116(8):1490-500.

d'Hellencourt CL, Harry GJ (2005) Molecular profiles of mRNA levels in laser capture microdissected murine hippocampal regions differentially responsive to TMT-induced cell death. J Neurochem 93(1):206-20.

Liu D, Wang Z, Liu S et al (2011) Anti-inflammatory effects of fluoxetine in lipopolysaccharide(LPS)-stimulated microglial cells. Neuropharmacology 61(4):592-9.

Lull ME, Block ML. (2010) Microglial activation and chronic neurodegeneration. Neurotherapeutics 7(4):354-65.

McPherson CA, Kraft AD, Harry GJ (2011) Injury-induced neurogenesis: consideration of resident microglia as supportive of neural progenitor cells. Neurotox Res 19(2):341-52.

Minghetti L, Ajmone-Cat MA, De Berardinis MA, De Simone R (2005) Microglial activation in chronic neurodegenerative

diseases: roles of apoptotic neurons and chronic stimulation. Brain Res Brain Res Rev 48(2):251-6.

Nieminen AL, Gores GJ, Bond JM et al (1992) A novel cytotoxicity screening assay using a multiwell fluorescence scanner. Toxicol Appl Pharmacol 115(2):147-55.

Nilsberth C, Kostyszyn B, Luthman J (2002) Changes in APP, PS1 and other factors related to Alzheimer's disease pathophysiology after trimethyltin-induced brain lesion in the rat. Neurotox Res 4(7-8):625-636.

Noraberg J, Gramsbergen JB, Fonnum F, Zimmer J (1998) Trimethyltin (TMT) neurotoxicity in organotypic rat hippocampal slice cultures. Brain Res 9;783(2):305-15.

Ogita K, Nitta Y, Watanabe M et al (2004) In vivo activation of c-Jun N-terminal kinase signaling cascade prior to granule cell death induced by trimethyltin in the dentate gyrus of mice. Neuropharmacology 47(4):619-30.

Raad H, Paclet MH, Boussetta T et al (2009) Regulation of the phagocyte NADPH oxidase activity: phosphorylation of gp91phox/NOX2 by protein kinase C enhances its diaphorase activity and binding to Rac2, p67phox, and p47phox. FASEB J 23(4):1011-22.

Park SJ, Lee JH, Kim HY et al (2012) Astrocytes, but not microglia, rapidly sense H_2O_2 via STAT6 phosphorylation,

resulting in cyclooxygenase-2 expression and prostaglandin release. J Immunol 15;188(10):5132-41.

Park SY, Jin ML, Kim YH et al (2012) Anti-inflammatory effects of aromatic-turmerone through blocking of NF-κB, JNK, and p38 MAPK signaling pathways in amyloid β-stimulated microglia. Int Immunopharmacol 14(1):13-20.

Peterson LJ, Flood PM (2012) Oxidative stress and microglial cells in Parkinson's disease. Mediators Inflamm 2012:401264.

Piacentini R, Gangitano C, Ceccariglia S et al (2008) Dysregulation of intracellular calcium homeostasis is responsible for neuronal death in an experimental model of selective hippocampal degeneration induced by trimethyltin. J Neurochem 1;105(6):2109-21.

Qing Y, Liang Y, Du Q et al (2013) Apoptosis induced by trimethyltin chloride in human neuroblastoma cells SY5Y is regulated by a balance and cross-talk between NF-κB and MAPKs signaling pathways. Arch Toxicol 87(7):1273-85.

Ransohoff RM, Perry VH (2009) Microglial physiology: unique stimuli, specialized responses. Annu Rev Immunol 27:119-45.

Reali C, Scintu F, Pillai R et al (2005) S100b counteracts effects of the neurotoxicant trimethyltin on astrocytes and microglia. J Neurosci Res 1;81(5):677-86.

Rosenstiel P, Lucius R, Deuschl G et al (2001) From theory to therapy: implications from an in vitro model of ramified microglia. Microsc Res Tech 1;54(1):18-25.

Roy A, Fung YK, Liu X, Pahan K (2006) Up-regulation of microglial CD11b expression by nitric oxide. J Biol Chem 26;281(21):14971-80.

Rozenfeld C, Martinez R, Figueiredo RT et al (2003) Soluble factors released by Toxoplasma gondii-infected astrocytes down-modulate nitric oxide production by gamma interferon-activated microglia and prevent neuronal degeneration. Infect Immun 71(4):2047-57.

Röhl C, Grell M, Maser E (2009) The organotin compounds trimethyltin (TMT) and triethyltin (TET) but not tributyltin (TBT) induce activation of microglia co-cultivated with astrocytes. Toxicol In Vitro 23(8):1541-7.

Röhl C, Sievers J (2005) Microglia is activated by astrocytes in trimethyltin intoxication. Toxicol Appl Pharmacol 1;204(1):36-45.

Solà C, Casal C, Tusell JM, Serratosa J (2002) Astrocytes enhance lipopolysaccharide-induced nitric oxide production by microglial cells. Eur J Neurosci 16(7):1275-83.

Stansley B, Post J, Hensley K (2012) A comparative review of cell culture systems for the study of microglial biology in Alzheimer's disease. J Neuroinflammation 31;9:115.

Steelman AJ, Li J (2014) Astrocyte galectin-9 potentiates microglial TNF secretion. J Neuroinflammation 27;11:144.

Tang X, Li N, Kang L et al (2013) Chronic low level trimethyltin exposure and the risk of developing nephrolithiasis. Occup Environ Med 70(8):561-7.

Vincent VA, Tilders FJ, Van Dam AM (1997) Inhibition of endotoxin-induced nitric oxide synthase production in microglial cells by the presence of astroglial cells: a role for transforming growth factor beta. Glia 19(3):190-8.

Viviani B, Corsini E, Galli CL, Marinovich M (1998) Glia increase degeneration of hippocampal neurons through release of tumor necrosis factor-alpha. Toxicol Appl Pharmacol 150(2):271-6.

Wakselman S, Béchade C, Roumier A et al (2008) Developmental neuronal death in hippocampus requires the microglial CD11b integrin and DAP12 immunoreceptor. J Neurosci 6;28(32):8138-43.

Wang X, Cai J, Zhang J et al (2008) Acute trimethyltin exposure induces oxidative stress response and neuronal apoptosis in Sebastiscus marmoratus. Aquat Toxicol 20;90(1):58-64.

Wilms H, Claasen J, Röhl C et al (2003) Involvement of benzodiazepine receptors in neuroinflammatory and

neurodegenerative diseases: evidence from activated microglial cells in vitro. Neurobiol Dis 14(3):417-24.

Xing B, Bachstetter AD, Van Eldik LJ (2011) Microglial p38α MAPK is critical for LPS-induced neuron degeneration, through a mechanism involving TNFα. Mol Neurodegener 20;6:84.

Yan L, Liu S, Wang C et al (2013) JNK and NADPH oxidase involved in fluoride-induced oxidative stress in BV-2 microglia cells. Mediators Inflamm 2013:895975.

Yoo CI, Kim Y, Jeong KS et al (2007) A case of acute organotin poisoning. J Occup Health 49(4):305-10.

Zhu L, Bi W, Lu D et al (2014) Luteolin inhibits SH-SY5Y cell apoptosis through suppression of the nuclear transcription factor-κB, mitogen-activated protein kinase and protein kinase B pathways in lipopolysaccharide-stimulated cocultured BV2 cells. Exp Ther Med 7(5):1065-1070.

국문 초록

유기주석 화합물 (organotin compound)의 일종인 trimethyltin (TMT)은 중추신경계, 특히 해마 신경세포의 사멸과 신경계의 기능손상을 유발할 수 있는 신경독성물질로 알려져 있다. TMT에 의한 선택적인 신경세포의 손상 기전은 아직 명확히 밝혀져 있지 않으나, 산화성 스트레스, 미세아교세포(microglia)의 활성화와 이에 따른 염증반응 등이 중요한 역할을 할 것으로 추정되고 있다. 한편 미세아교세포의 활성화는 TMT 신경독성의 병리학적 특징의 하나로 잘 알려져 있으나, TMT가 미세아교세포를 어떤 기전으로 활성화시키는 지에 대한 연구는 제한적이다. 그러므로 본 연구에서는 TMT에 의한 미세아교세포의 활성화 기전을 알아보고자 하였다. 미세아교세포주인 BV-2 cell을 이용하여 TMT 처리 후 세포 내 활성산소(ROS)의 생성, 신호전달 경로의 활성화(MAPKs, NF-κB), nitric oxide (NO) 그리고 TNF-α 유리를 확인하였다. 또한 해마 신경세포주인 HT22 cell를 BV-2 cell과 공동배양(co-culture)하여 TMT에 의한 BV-2 cell의 활성화가 신경세포의 생존에 미치는 영향도 검토하였다. 실험 결과 TMT는 BV-2 cell에서 활성산소의 생성을 증가시키고, JNK와 p38 MAPKs의 인산화 유도와 NF-κB의 활성화 및 CD11b의 발현이 증가되는 결과를 얻었다. 그리고 TMT 처리는 BV-2 cell에서 NO와 TNF-α의 유리를 증가시켰다. NADPH oxidase 억제제인 apocynin을 전처리한 경우 TMT에 의한 활성산소의 생성 이외에도 활성화되는 신호전달경로(p38, JNK 그리고 NF-κB), 그리고 NO와 TNF-α 유리가 효과적으로 억제되는 것을 확인할 수 있었다. 한편 BV-2 cell과 HT22 cell 공동배양 조건에서는 TMT는 BV-2 cell을 활성화시켜 HT22 cell의 세포사를 초래하였다. 그리고 동일 조건에서 apocynin 그리고 SB203580 (p38 억제제), SP600125 (JNK 억제제) 를 전처리한

경우 BV-2 cell에 의한 HT22 cell의 세포사를 유의하게 억제하였다.

이상의 결과는 TMT는 BV-2 cell을 활성산소의 생성을 통한 MAPKs, NF-κB 경로를 직접 활성화시키고, 그 결과 NO, TNF-α 유리를 증가시킬 수 있으며, 유리된 NO, TNF-α 그리고 활성산소가 복합적으로 작용하여 HT22 cell의 세포사를 초래할 수 있음을 확인한 것이다.

주요어 : BV-2 미세아교세포주, HT22 neuroblastoma cells, mitogen-activated protein kinases (MAPKs), NADPH oxidase , nuclear factor κB (NF-κB, trimethyltin (TMT)

학 번 : 2013-21720